Effect of Conformational Constraints on Gated Electron-Transfer Kinetics. A Multifaceted Study on Copper(II/I) Complexes with *cis*- and *trans*-Cyclohexanediyl-[14]aneS$_4$

Cynthia A. Salhi,[1a] Qiuyue Yu,[1a] Mary Jane Heeg,[1a] Nicole M. Villeneuve,[1a] Kerri L. Juntunen,[1a] Ronald R. Schroeder,[1a] L. A. Ochrymowycz,[1b] and D. B. Rorabacher*[,1a]

Departments of Chemistry, Wayne State University, Detroit, Michigan 48202, and University of Wisconsin—Eau Claire, Eau Claire, Wisconsin 54701

Received October 13, 1994[⊗]

A multifaceted study has been conducted on the electron-transfer reactions of the copper(II/I) complexes formed with 2,3-*cis*- and 2,3-*trans*-cyclohexanediyl-1,4,8,11-tetrathiacyclotetradecane (designated as *cis*- and *trans*-cyhx-[14]aneS$_4$). Each system has been studied by (i) ^{1}H-NMR line broadening in D_2O to determine the electron self-exchange rate constants at zero driving force, (ii) rapid-scan cyclic voltammetry in 80% methanol−20% water (w/w) to determine the rate constants for conformational changes and heterogeneous electron transfer, and (iii) stopped-flow spectrophotometry using a total of eight oxidizing and reducing counterreagents to determine the cross-reaction electron-transfer rate constants from which self-exchange rate constants can be calculated for various driving forces. The crystal structures of both Cu^{II}L complexes and of Cu^{I}(*trans*-cyhx-[14]aneS$_4$) have also been determined. From the NMR measurements, the electron self-exchange rate constants have been evaluated [at 25 °C, μ = 0.10 M (NO_3^-)] as $k_{11(ex)} = (5.0 \pm 0.5) \times 10^4$ and $\leq 10^3$ M^{-1} s^{-1} for Cu$^{II/I}$(*cis*-) and Cu$^{II/I}$(*trans*-cyhx-[14]aneS$_4$), respectively. Application of the Marcus relationship to the numerous cross-reaction rate constants yields variable behavior which is consistent with a dual-pathway mechanism for which the following self-exchange rate constants have been resolved [25 °C, μ = 0.10 M (ClO_4^-)]: for Cu$^{II/I}$(*cis*-cyhx-[14]aneS$_4$), $k_{11(A)} = 5 \times 10^4$, $k_{11(B)} \leq 10$ M^{-1} s^{-1}; for Cu$^{II/I}$(*trans*-cyhx-[14]aneS$_4$), $k_{11(A)} = 2 \times 10^3$, $k_{11(B)} \leq 10$ M^{-1} s^{-1}. The reduction reactions proceed by the most favorable pathway (pathway A) involving a metastable Cu^{I}L intermediate (P) while the limiting oxidation reactions proceed by an alternate pathway (pathway B) involving a less stable Cu^{II}L intermediate (Q). The change in pathway is mediated by the rate constant (k_{RP}) for the formation of the Cu^{I}L(P) intermediate from the stable Cu^{I}L(R) complex. This latter rate constant has been estimated from both cyclic voltammetric measurements (CV, 80% methanol) and Cu^{I}L homogeneous oxidation kinetics (Ox, H_2O) as follows [25 °C]: for Cu^{I}(*cis*-cyhx-[14]aneS$_4$), $k_{RP} = 4.4 \times 10^2$ (CV) and 1.1×10^2 s^{-1} (Ox); for Cu^{I}(*trans*-cyhx-[14]-aneS$_4$), $k_{RP} = 1.5 \times 10^2$ (CV) and 32 s^{-1} (Ox). The values obtained from homogeneous oxidations are believed to be the more reliable. The crystal structures reveal that both Cu^{II}L complexes are square pyramidal with the four sulfur donor atoms occupying the basal plane and a coordinated water molecule (or anion) at the apex. The Cu^{I}(*trans*-cyhx-[14]aneS$_4$) complex is in a flattened tetrahedral geometry in which all four sulfur donor atoms remain coordinated. These structures imply that, for each Cu$^{II/I}$L system, two sulfur donor atoms must invert during the overall electron-transfer process. It is postulated that these donor atom inversions may represent the primary barrier for the conformational change represented in the R → P step. The self-exchange rate constant representative of the electron-transfer step itself, corrected for the separate conformational change step, is estimated to be on the order of 10^6 M^{-1} s^{-1} for both systems, equivalent to the largest self-exchange rate constants known for rigid Cu$^{II/I}$L systems. Crystal data [Mo Kα radiation (λ = 0.710 73 Å)] are as follows. For [Cu^{II}(*cis*-cyhx-[14]aneS$_4$)(H_2O)](ClO_4)$_2$ (**1**): $CuS_4C_{14}H_{28}Cl_2O_9$, triclinic system, space group $P\bar{1}$, a = 9.734(4) Å, b = 10.155-(3) Å, c = 13.058(4) Å, α = 91.73(2)°, β = 91.52(3)°, γ = 117.75(3)°, V = 1140.6(7) Å^3, Z = 2, R = 0.049, R_w = 0.050, T = −110 °C. For [Cu^{II}(*trans*-cyhx-[14]aneS$_4$)(H_2O)](ClO_4)$_2$ (**2a**): $CuS_4C_{14}H_{28}Cl_2O_9$, triclinic system, space group $P\bar{1}$, a = 9.177(5) Å, b = 10.641(5) Å, c = 13.037(4) Å, α = 87.26(3)°, β = 88.13 (4)°, γ = 69.19(3)°, V = 1188.5(8) Å^3, Z = 2, R = 0.050, R_w = 0.056, T = −110 °C. For [Cu^{II}(*trans*-cyhx-[14]aneS$_4$)Cl]·$^1/_2$$CuCl_4$·$H_2O$ (**2b**): $Cu_{1.5}C_{14}H_{28}S_4Cl_3O$, orthorhombic system, space group *Pbcn*, a = 28.206(7) Å, b = 10.115-(3) Å, c = 14.707(2) Å, V = 4196(2) Å^3, Z = 8, R = 0.038, R_w = 0.042, T = 22 °C. For [Cu^{I}(*trans*-cyhx-[14]-aneS$_4$)]ClO_4·$^1/_4$$H_2O$ (**3**): $CuS_4C_{14}H_{26.5}ClO_{4.25}$, monoclinic system, space group $P2_1/n$, a = 10.135(2) Å, b = 16.044(2) Å, c = 12.675(2) Å, β = 105.10(1)°, V = 1989.9(5) Å^3, Z = 4, R = 0.038, R_w = 0.038, T = −110 °C.

Introduction

Gated electron transfer, as applied to redox systems, refers to a process in which the rate of electron transfer is ultimately limited *in one direction only* by the rate of conformational change in one of the reacting species. It has been postulated that such processes may be particularly important in biological systems where the gating phenomenon may hinder the contribution of undesirable back-reactions.[2] Although the number of systems in which gated electron-transfer behavior has been thoroughly documented is small, there are a number of biological and inorganic electron-transfer reactions for which some evidence exists that conformational changes are rate limiting for either the Cu(II/I)[3] or the Fe(III/II) redox couple.[4]

[⊗] Abstract published in *Advance ACS Abstracts,* October 15, 1995.

(1) (a) Wayne State University. (b) University of Wisconsin—Eau Claire.

(2) Hoffman, B. M.; Ratner, M. A. *J. Am. Chem. Soc.* **1987**, *109*, 6237−6243.

0020-1669/95/1334-6053$09.00/0

Scheme 1

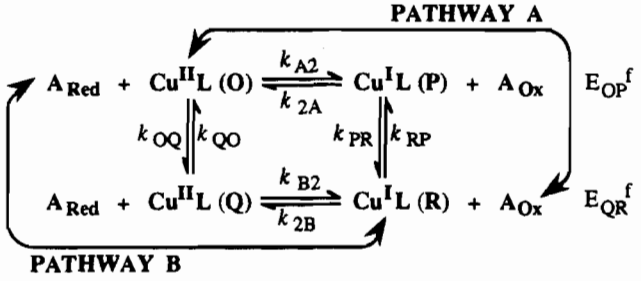

We have previously noted[5] that Cu(II/I) systems are prime candidates for gated electron transfer since the coordination geometries preferred by the Cu(II) and Cu(I) oxidation states differ significantly, the oxidant preferring six-coordinate tetragonal or five-coordinate square pyramidal (or trigonal bipyramidal) geometries while the reductant tends to prefer four-coordinate tetrahedral arrangements.[6] Thus, the electron-transfer process in these systems is generally accompanied by one- or two-coordinate bond formations (or ruptures) and a change in ligand conformation.

In recent studies on the cross-reaction electron-transfer kinetics of Cu(II/I) complexes formed with macrocyclic tetrathiaethers,[5,7-10] we were able to provide convincing evidence for the existence of a dual-pathway square scheme (Scheme 1) in which the electron-transfer step and conformational change occur sequentially, rather than concertedly. In this mechanism, $Cu^{II}L(O)$ and $Cu^{I}L(R)$ are the thermodynamically stable oxidant and reductant whereas $Cu^{II}L(Q)$ and $Cu^{I}L(P)$ are metastable intermediates. In all of the systems which we have studied to date, the preferred pathway is pathway A, in which, for the $Cu^{II}L$ reduction, the step involving conformational change occurs *after* the electron-transfer step. In corroboration of this, the onset of gated (first-order) behavior has been observed only for very fast *oxidation* reactions where the conformational change *preceding* the electron-transfer step becomes rate limiting. On the basis of the kinetics observed under gated conditions, the k_{RP} rate constant for the conformational change itself has been evaluated for the complexes formed with [14]aneS$_4$[7] and *syn*- and *anti*-[14]aneS$_4$-diol[9] (Figure 1). Limiting estimates have also been obtained for the Cu(II/I) systems with [13]aneS$_4$ and [15]aneS$_4$[8] (Figure 1). For the $Cu^{II/I}$([14]aneS$_4$) system we have also been able to utilize rapid-scan cyclic voltammetry to obtain an independent measurement of k_{RP} as well as the other stepwise rate constants involved in the dual-pathway scheme.[11]

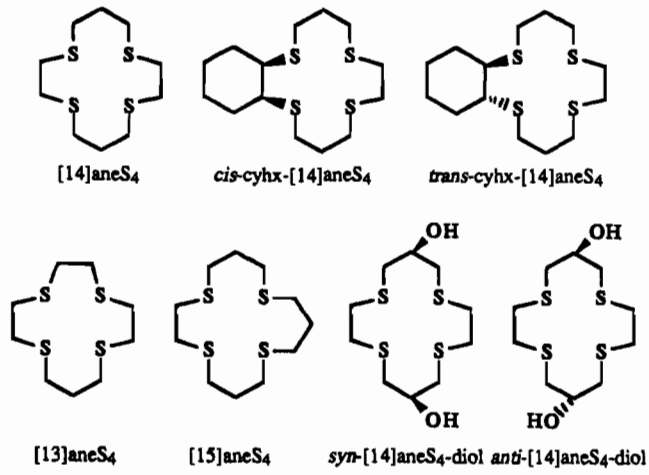

Figure 1. Ligands discussed in this work.

From the inherent nature of gated behavior, the conformational change itself should reflect the influence of the coordinated ligand upon the reorganizational barrier. To date, however, conformational change rate constants have not been correlated to specific ligand constraints. In the current study, we have investigated the electron-transfer kinetics of two modified systems in which one of the ethylene bridges in the [14]aneS$_4$ ligand has been replaced by either *cis*- or *trans*-1,2-cyclohexane to yield ligands designated as *cis*- and *trans*-cyhx-[14]aneS$_4$ (Figure 1). The properties of the Cu(II) complexes formed with these two ligands were recently studied both in 80% methanol and in acetonitrile.[12] In each case, the stability constant is about 50 times larger than that for the parent Cu^{II}([14]aneS$_4$) complex, suggesting that the cyclohexanediyl substituents introduce significant constraints into the 14-membered macrocycle. Subsequent complex formation and dissociation kinetic measurements have shown that the increase in the $Cu^{II}L$ stability constants (Table 1) observed for these and related cyclohexanediyl derivatives is entirely due to a decrease in the dissociation rate constant.[13] Molecular mechanics calculations

(3) (a) Kostic, N. M.; *Abstracts of Papers*, 205th National Meeting of the American Chemical Society, Denver, CO, March 28–April 2, 1993; American Chemical Society: Washington, DC, 1993; INOR 261. (b) Zhou, J. S.; Kostic, N. M. *J. Am. Chem. Soc.* **1993**, *115*, 10796–10804. (c) Qin, L.; Kostic, N. *Biochemistry* **1993**, *32*, 6073–6080. (d) Lappin, A. G.; Lewis, C. A.; Ingledew, C. A. *Inorg. Chem.* **1985**, *24*, 1446–1450. (e) Allan, A. E.; Lappin, A. G.; Laranjeira, M. C. M. *Inorg. Chem.* **1984**, *23*, 477–482. (f) Davies, K. M. *Inorg. Chem.* **1983**, *22*, 615–619. (g) Leupin, P.; Al-Shatti, N.; Sykes, A. G. *J. Chem. Soc., Dalton Trans.* **1982**, 927–930. (h) Al-Shatti, N.; Lappin, A. G.; Sykes, A. G. *Inorg. Chem.* **1981**, *20*, 1466–1469. (i) Silvestrini, M. C.; Brunori, M.; Wilson, M. T.; Darley-Usmar, V. M. *J. Inorg. Biochem.* **1981**, *14*, 327–338. (j) Rosen, P.; Pecht, I. *Biochemistry* **1976**, *15*, 775–786. (k) Wilson, M. T.; Greenwood, C.; Brunori, M.; Antonini, E. *Biochem. J.* **1975**, *145*, 449–457.

(4) (a) Qin, L.; Kostic, N. *Biochemistry* **1994**, *33*, 12592–12599. (b) Feitelson, J.; McLendon, G. *Biochemistry* **1991**, *30*, 5051–5055. (c) Walker, M. C.; Tollin, G. *Biochemistry* **1991**, *30*, 5546–5555. (d) Wallin, S. A.; Stemp, E. D. A.; Everest, A. M.; Nocek, J. M.; Netzel, T. L.; Hoffman, B. M. *J. Am. Chem. Soc.* **1991**, *113*, 1842–1844. (e) Nocek, J. M.; Liang, N.; Wallin, S. A.; Mauk, A. G.; Hoffman, B. M. *J. Am. Chem. Soc.* **1990**, *112*, 1623–1625. (f) Zang, L.-H.; Maki, A. H. *J. Am. Chem. Soc.* **1990**, *112*, 4346–4351. (g) Isied, S. S. *Electron Transfer in Biology and the Solid State*; Johnson, M. K., King, R. B., Kurtz, D. M., Jr., Kutal, C., Norton, M. L., Scott, R. A., Eds.; American Chemical Society: Washington, DC, 1990; pp 91–100. (h) Hazzard, J. T.; McLendon, G.; Cusanovich, M. A.; Tollin, G. *Biochem. Biophys. Res. Commun.* **1988**, *151*, 429–434. (i) Malmstrom, B. G.; Nilsson, T. *Ann. N.Y. Acad. Sci.* **1988**, *550*, 177–184. (j) Wilson, M. T.; Allene, T.; Clague, M.; Conroy, K.; El-Agez, B. *Ann. N.Y. Acad. Sci.* **1988**, *550*, 167–176. (k) Bechtold, R.; Kuehn, C.; Lepre, C.; Isied, S. S. *Nature* **1986**, *322*, 286–288.

(5) (a) Martin, M. J.; Endicott, J. F.; Ochrymowycz, L. A.; Rorabacher, D. B. *Inorg. Chem.* **1987**, *26*, 3012–3022. (b) Rorabacher, D. B.; Meagher, N. E.; Juntunen, K. L.; Robandt, P. V.; Leggett, G. H.; Salhi, C. A.; Dunn, B. C.; Schroeder, R. R.; Ochrymowycz, L. A. *Pure Appl. Chem.* **1993**, *65*, 573–578.

(6) (a) Hathaway, B. J. *Coord. Chem. Rev.* **1981**, *35*, 211–252. (b) Hathaway, B. J.; Billing, D. E. *Coord. Chem. Rev.* **1970**, *5*, 143–207.

(7) Meagher, N. E.; Juntunen, K. L.; Salhi, C. A.; Ochrymowycz, L. A.; Rorabacher, D. B. *J. Am. Chem. Soc.* **1992**, *114*, 10411–10420.

(8) Leggett, G. H.; Dunn, B. C.; Vande Linde, A. M. Q.; Ochrymowycz, L. A.; Rorabacher, D. B. *Inorg. Chem.* **1993**, *32*, 5911–5918.

(9) Meagher, N. E.; Juntunen, K. L.; Heeg, M. J.; Salhi, C. A.; Dunn, B. C.; Ochrymowycz, L. A.; Rorabacher, D. B. *Inorg. Chem.* **1994**, *33*, 670–679.

(10) Dunn, B. C.; Ochrymowycz, L. A.; Rorabacher, D. B. *Inorg. Chem.* **1995**, *34*, 1954–1956.

(11) (a) Robandt, P. V.; Schroeder, R. R.; Rorabacher, D. B. *Inorg. Chem.* **1993**, *32*, 3957–3963. (b) Bernardo, M. M.; Robandt, P. V.; Schroeder, R. R.; Rorabacher, D. B. *J. Am. Chem. Soc.* **1989**, *111*, 1224–1231.

(12) Aronne, L.; Dunn, B. C.; Vyvyan, J. R.; Souvignier, C. W.; Mayer, M. J.; Howard, T. A.; Salhi, C. A.; Goldie, S. N.; Ochrymowycz, L. A.; Rorabacher, D. B. *Inorg. Chem.* **1995**, *34*, 357–369.

(13) Aronne, L.; Yu, Q.; Ochrymowycz, L. A.; Rorabacher, D. B. *Inorg. Chem.* **1995**, *34*, 1844–1851.

Table 1. Physical Properties of the Cu(II/I) Systems with [14]aneS$_4$, *cis*-cyhx-[14]aneS$_4$, and *trans*-cyhx-[14]aneS$_4$ in Aqueous Solution at 25 °C, $\mu = 0.10$ M[a]

	Cu(II/I) complex system		
physical property	[14]aneS$_4$	*cis*-cyhx-[14]aneS$_4$	*trans*-cyhx-[14]aneS$_4$
Cu^{II}L max abs peaks: λ, nm	390, 570	390, 570	388, 558
molar absorptivity: $10^{-3}\,\epsilon$, M^{-1} cm^{-1}	8.0, 1.9	7.4, 2.0	8.9, 1.8
formal potential: E^f, V vs NHE	0.58	0.53$_6$	0.60$_0$
contact radius: r, nm	0.44	0.44	0.44
Cu^{II}L stability constant, M^{-1} (80% CH$_3$OH)	3.0×10^3	1.61×10^5	1.12×10^5
Cu^{I}L stability constant, M^{-1} (80% CH$_3$OH)	1.2×10^{11}	1.2×10^{12}	9.9×10^{12}

[a] All data from ref 12.

indicate that this decrease is attributable to an increase in strain energies for some of the reaction intermediates as the ligands undergo conformational change prior to the rupture of the Cu−S bonds.[13] Since the ligand contortions in the early stages of dissociation are very similar to the conformational changes which must accompany electron transfer in the Cu(II/I) systems, we initially surmised that the conformational changes associated with Cu^{I}L oxidation might also become more sluggish with the introduction of the cyclohexanediyl substituents and, therefore, that the onset of gated behavior would be more easily observed.

In the current work, we have undertaken an exceptionally thorough investigation of the electron-transfer kinetics of the Cu$^{II/I}$(*cis*-cyhx-[14]aneS$_4$) and Cu$^{II/I}$(*trans*-cyhx-[14]aneS$_4$) systems including the use of NMR line-broadening measurements, rapid-scan cyclic voltammetry, and stopped-flow kinetic measurements on the homogeneous electron-transfer reactions of these systems with eight reducing and oxidizing counterreagents. The crystal structures of both Cu^{II}L complexes and of Cu^{I}(*trans*-cyhx-[14]aneS$_4$) have also been determined. The resulting behavior is examined in light of the various intermediate conformations which are presumed to be formed during the overall electron-transfer process.

Experimental Section

Reagents. The syntheses of both the *cis*- and *trans*-cyhx-[14]aneS$_4$ ligands have been previously described.[12] For the Cu(II) complexes in aqueous solution, the major visible absorbance peaks and their molar absorptivities as well as the Cu$^{II/I}$L potentials are listed in Table 1.[12] The reagent [Co(bpy)$_3$](ClO$_4$)$_3$·3H$_2$O was prepared by the method of Burstall and Nyholm.[14] Solutions prepared from this material were standardized spectrophotometrically using the molar absorptivity values reported by Martin and Waind.[15] The Co(III) compound was then reduced over copper shot for 1 h to generate the Co(II) species which was used immediately. The synthetic procedures and solution preparations of the other four reducing agents and of the three oxidizing agents used in this work have been previously referenced.[5a,7]

Solutions and Instrumentation. Solutions of the Cu(II) complexes with both *cis*- and *trans*-cyhx-[14]aneS$_4$ were prepared by dissolving the ligand in an excess of purified Cu(ClO$_4$)$_2$ solution and were standardized spectrophotometrically. Solutions of the Cu(I) complexes were prepared by placing the Cu^{II}L solutions over copper shot under a nitrogen atmosphere. For the cross-reaction kinetic measurements, the ionic strength was controlled using 0.10 M HClO$_4$ while 0.10 M DNO$_3$ was used for the NMR measurements. All other procedures and instrumentation for both the stopped-flow kinetic measurements and the NMR line-broadening measurements were identical to those described for our earlier studies.[7] Slow-scan cyclic voltammetric (CV) measurements (0.01−1.0 V s^{-1}) were made with a Bioanalytical Systems electrochemical analyzer, Model BAS 100 (BAS, Lafayette, IN). A glassy carbon electrode (BAS, Lafayette, IN) was used as the working electrode because of its wider positive potential range and the decreased tendency of the Cu^{I}L complexes to adsorb on the electrode surface (compared to Pt, Ag, Au, or Hg electrodes). Rapid-scan CV was conducted using an ultramicro glassy carbon working electrode (10 μm diameter) and a miniature Ag/AgCl reference electrode filled with saturated NaCl, along with a platinum wire auxiliary electrode (all from Cypress Systems, Lawrence, KS). The instrumentation for the rapid-scan CV measurements was fabricated in our laboratory using adaptations of Saveant's design,[16] for which sweep rates up to 100 kV s^{-1} were achievable.[17] In practice, the development of large background currents restricted the usable sweep rates to under 10 kV s^{-1} for the systems studied in this work. Prior to each CV scan, the glassy carbon electrode was polished using the protocol previously described.[11b] This was followed by sonication to remove any surface particles.

Crystallography. Single-crystal X-ray diffraction measurements were performed on a Nicolet R3 automated diffractometer with Mo Kα radiation and a graphite monochromator. Experimental crystallographic data are presented in Table 2 and in the Supporting Information. All four structures reported in this work were solved by Patterson methods and refined in a full matrix with the programs of SHELX-76.[18] Neutral-atom scattering factors and corrections for anomalous dispersion were taken from standard tables.[19]

Crystals of [Cu^{II}(*cis*-cyhx-[14]aneS$_4$)(H$_2$O)](ClO$_4$)$_2$ (**1**), [Cu^{II}(*trans*-cyhx-[14]aneS$_4$)(H$_2$O)](ClO$_4$)$_2$ (**2a**), and [Cu^{I}(*trans*-cyhx-[14]aneS$_4$)]ClO$_4$·$^1/_4$H$_2$O (**3**) suitable for X-ray analysis were obtained by evaporation of the appropriate Cu(ClO$_4$)$_2$−ligand mixtures from 80% methanol. A crystal of Cu^{II}(*trans*-cyhx-[14]aneS$_4$)Cl]·$^1/_2$CuCl$_4$·H$_2$O (**2b**) was obtained by evaporation of a mixture of CuCl$_2$ and ligand from methylene chloride/acetonitrile.

Results

Determination of Cu$^{II/I}$L Potential Values. The aqueous formal potential values of the two Cu$^{II/I}$L redox couples were determined by cyclic voltammetry (CV) at ambient temperature in 0.10 M NaClO$_4$ at slow scan rates ranging from 0.1 to 0.5 V s^{-1}. The CV curves were well behaved, and although there was some evidence of quasi-reversibility in the case of the *trans*-cyclohexanediyl derivative, constant values of $E_{1/2}$ were obtained over the scan range sampled. The experimentally determined potential values are included (as formal potentials) in Table 1, where they are compared to those for the Cu$^{II/I}$([14]aneS$_4$) system.

NMR Line-Broadening Measurements. The ^{1}H spectrum of the uncomplexed *cis*-cyhx-[14]aneS$_4$ ligand in CD$_3$Cl is illustrated in Figure 2A. Several homonuclear decoupling experiments and a heteronuclear 2D experiment permitted the identification of all peaks as identified in the figure. Due to conformational changes in the cyclohexyl ring which are occurring within the NMR time scale, broad bands are produced by the A, A′, and B protons. The ^{1}H spectrum of the Cu^{I}L complex in D$_2$O is shown in Figure 2B. The peak assignments have been made by analogy to the spectrum of the free ligand. It was not possible to verify the assignments through decoupling experiments because of the broad unresolved peaks. This latter spectrum is temperature dependent: at 25 °C, the spectrum indicates a conformational exchange which is slow on the NMR time scale; in the range of 55−75 °C, the rate of this

(14) Burstall, F. H.; Nyholm, R. S. *J. Chem. Soc.* **1952**, 3570−3579.
(15) Martin, B.; Waind, G. M. *J. Chem. Soc.* **1958**, 4284−4288.
(16) (a) Saveant, J. M.; Garreau, D.; Hapilot, P. *J. Electroanal. Chem. Interfacial. Electrochem.* **1988**, *243*, 321−335. (b) *Ibid.* **1988**, *248*, 447−4501. (c) *Ibid.* **1989**, *272*, 1−16.
(17) Details of the rapid-scan instrumental design are provided in: Villeneuve, N. M., Ph.D. Dissertation, Wayne State University, 1995.
(18) Sheldrick, G. M. SHELX-76. University Chemical Laboratory, Cambridge, England, 1976.
(19) *International Tables for X-Ray Crystallography*; Kynoch: Birmingham, England, 1974; Vol. 4 (present distributor: D. Reidel, Dordrecht, The Netherlands).

Table 2. Crystallographic Data for $[Cu^{II}(cis\text{-cyhx-}[14]aneS_4)(OH_2)](ClO_4)_2$ (**1**), $[Cu^{II}(trans\text{-cyhx-}[14]aneS_4)(OH_2)](ClO_4)_2$ (**2a**), $[Cu^{II}(trans\text{-cyhx-}[14]aneS_4)Cl]\cdot{}^1/_2CuCl_4\cdot H_2O$ (**2b**), and $[Cu^{I}(trans\text{-cyhx-}[14]aneS_4)]ClO_4\cdot{}^1/_4H_2O$ (**3**)

	1	**2a**	**2b**	**3**
formula	$CuC_{14}H_{28}S_4Cl_2O_9$	$CuC_{14}H_{28}S_4Cl_2O_9$	$Cu_{1.5}C_{14}H_{28}S_4Cl_3O$	$CuC_{14}H_{26.5}S_4ClO_{4.25}$
fw	603.08	603.08	542.31	490.12
space group	$P\bar{1}$	$P\bar{1}$	*Pbcn* (No. 60)	$P2_1/n$
a, Å[a]	9.734(4)	9.177(5)	28.206(7)	10.135(2)
b, Å[a]	10.155(3)	10.641(5)	10.115(3)	16.044(2)
c, Å[a]	13.058(4)	13.037(4)	14.707(2)	12.675(2)
α, deg[a]	91.73(2)	87.26(3)	90	90
β, deg[a]	91.52(3)	88.13(4)	90	105.10(1)
γ, deg[a]	117.75(3)	69.19(3)	90	90
V, Å^3	1140.6(7)	1188.5(8)	4196(2)	1989.9(5)
Z	2	2	8	4
ρ(calc), g cm^{-3}	1.756	1.685	1.717	1.636
γ, Å	0.710 73	0.710 73	0.710 73	0.710 73
T, °C	−110	−110	22	−110
μ, cm^{-1}	15.90	15.26	23.09	16.56
transm factors[b]			0.573−0.498	
R	0.049	0.050	0.038	0.038
R_w	0.050	0.056	0.042	0.038

[a] Cell constants were calculated from 25 high angle ($2\theta > 20°$) reflections. [b] No absorption corrections were made on the low-temperature data sets.

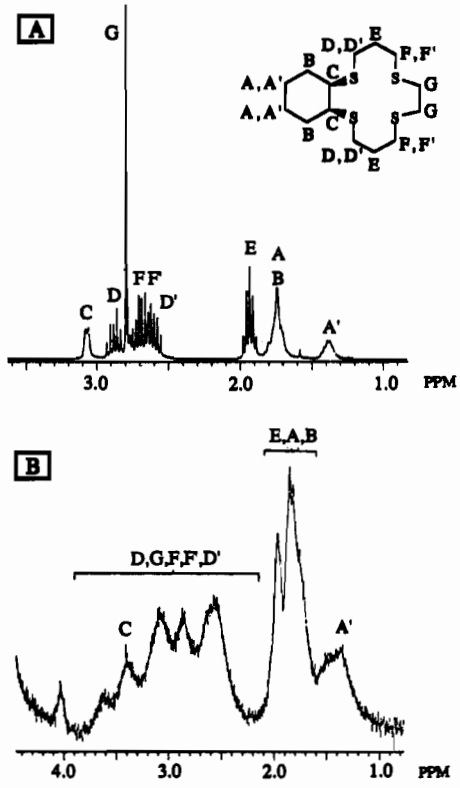

Figure 2. (A) ^{1}H-NMR spectrum for uncomplexed *cis*-cyhx-[14]aneS$_4$ in $CDCl_3$. (B) ^{1}H-NMR spectrum for Cu^I(*cis*-cyhx-[14]aneS$_4$) in D_2O. Spectral assignments are based on homonuclear decoupling and heteronuclear 2D experiments on the uncomplexed ligand.

conformational change increases such that the peaks begin to sharpen. In addition, nearly all peaks shift further downfield as the temperature is elevated.

Upon the addition of $Cu^{II}L$ to a solution containing $Cu^{I}L$, the $Cu^{I}L$ NMR peaks broaden perceptibly as a result of electron self-exchange:

$$*Cu^{I}L + Cu^{II}L \overset{k_{11(ex)}}{\rightleftharpoons} *Cu^{II}L + Cu^{I}L \qquad (1)$$

In view of the large contribution of conformational change to the observed band width in the vicinity of room temperature, the line-broadening experiments were performed at 55, 65, and 75 °C. The monitored peaks were those in the range 2.5−3.2 ppm (Figure 2B), attributed to the D, D′, F, F′, and G protons. In the elevated temperature region used for making the line-broadening measurements, these peaks are further downfield at 3.0−3.7 ppm and combine to give the appearance of a distorted doublet. The contribution of the conformational changes was still appreciable within the monitored temperature range, and with the spectral complexity arising from the numerous contributing proton environments, the peaks tended to be excessively broad, leading to a lower signal-to-noise ratio. Moreover, the complexity of the overlapping peaks made it difficult to achieve an accurate deconvolution. The best visual fit to the experimental spectra was obtained by treating the spectral region of interest as arising from three overlapping peaks with relative areas of 4:2:6.

After the optimum conditions for line width measurements were identified, a series of solutions was prepared in D_2O, utilizing the methods previously described,[7,20,21] in which a constant concentration of $Cu^{I}L$ was maintained with varying amounts of added $Cu^{II}L$. Excess aquacopper(II) ion (2.63 mM) was also added to prevent the dissociation of $Cu^{II}L$.[22] (The paramagnetic line broadening arising from the aquacopper(II) ion itself was constant, and the contributions from the low levels of added $Cu^{II}L$ were insignificant).[20,21] The solutions contained 0.10 M DNO_3 for ionic strength control; two additional measurements were made using 0.10 M $NaNO_3$ (pD ≪ 5) instead of DNO_3 to make certain that acidity had no influence on these measurements.[23] The data were treated using the method of McConnell and Berger:[24]

$$W_{DP}Q\pi = W_{D}Q\pi + k_{11(ex)}[Cu^{II}L] \qquad (2)$$

In this expression, W_D and W_{DP} represent the line widths for solutions containing only the diamagnetic species ($Cu^{I}L$) and a

(20) Vande Linde, A. M. Q.; Juntunen, K. L.; Mols, O.; Ksebati, M. B.; Ochrymowycz, L. A.; Rorabacher, D. B. *Inorg. Chem.* **1991**, *30*, 5037−5042.
(21) Vande Linde, A. M. Q.; Westerby, B. C.; Ochrymowycz, L. A.; Rorabacher, D. B. *Inorg. Chem.* **1993**, *32*, 251−257.
(22) The stability constant for the Cu^{II}(*cis*-cyhx-[14]aneS$_4$) complex is presumed to be greater than 10^6 M^{-1} in aqueous solution.[12] Therefore, the addition of 2 mM Cu^{II}_{aq} ensures that less than 0.1% of the total ligand will be uncomplexed.
(23) In ≥1 M HNO_3, nitric acid has been observed to oxidize the macrocyclic polythiaether ligands.
(24) McConnell, H. M.; Berger, S. B. *J. Chem. Phys.* **1957**, *27*, 230−234. Cf.: Gutowsky, H. S.; McCall, H. S.; Slichter, C. P. *J. Chem. Phys.* **1953**, *21*, 279−292.

Table 3. NMR Line-Broadening Data for $Cu^{II/I}$(*cis*-cyhx-[14]aneS$_4$) in D_2O as a Function of Temperature at $\mu = 0.10$ (DNO_3): [$Cu^{I}L$] = 1.40 mM, [Cu^{II}_{aq}] = 2.63 mM

	55 °C		65 °C		75 °C	
[$Cu^{II}L$], mM	width, Hz	$WQ\pi$, Hz	width, Hz	$WQ\pi$, Hz	width, Hz	$WQ\pi$, Hz
0.0264	42.57	131.2				
0.0368	43.33	133.5				
0.0502	43.71	134.7				
0.0532	43.71	134.7				
0.198	49.53	152.5	45.59	140.3	41.70	128.3
0.302	53.14	163.5	51.80	159.4	51.98	159.8
0.379	56.07	172.5	52.21	160.6	55.05	169.2
0.454	62.22	191.3	60.40	185.6	60.55	186.0
0.501	61.89	190.2	63.45	195.0		
$k_{11(ex)}$	1.269(52) × 10^5		1.762(261) × 10^5		2.185(255) × 10^5	

$\Delta H^{\ddagger} = 23(3)$ kJ mol^{-1}; $\Delta S^{\ddagger} = -77(8)$ J mol^{-1} K^{-1}
Extrapolated to 25 °C: $k_{11(ex)} = 5.0(5) \times 10^4$ M^{-1} s^{-1}

mixture of diamagnetic and paramagnetic species, respectively, and Q represents an ionic strength correction as previously described.[7,20,21] The results for all three temperatures are compiled in Table 3. The resulting activation parameters were utilized to estimate the value applicable to 25 °C: $k_{11} = 5.0$ ($\pm$0.5) × 10^4 M^{-1} s^{-1}.

The ^{1}H NMR spectrum for the uncomplexed *trans*-cyhx-[14]-aneS$_4$ ligand in CD_3OD is illustrated in Figure 3A. In the comparison of this spectrum to that for the *cis* ligand, a loss of molecular symmetry is evident, as shown by a broadening of most of the peaks as well as the disappearance of the sharp singlet at 2.8 ppm (proton G). In Figure 3A, this is replaced by a triplet which results from a coupling of the doublets for the G and G′ protons. The E protons produce a more complicated peak pattern, suggesting that these protons have become nonequivalent or that the D, D′, F and F′, protons no longer act simultaneously to give the peak multiplicity. Finally, the change in the shape of the peak at 1.6 ppm and the appearance of an additional peak at 2.15 ppm are indicative of asymmetry within the cyclohexyl ring.

The ^{1}H spectrum of the Cu^{I}(*trans*-cyhx-[14]aneS$_4$) complex in D_2O is shown in Figure 3B. The sharp peaks in this spectrum are in marked contrast to the appearance of the *cis* complex. The spectrum was found to be independent of temperature over the range 20−75 °C. Thus, the complex appears to form a stable conformation which does not change on the NMR time scale ($\ll 10^3$−10^6 s^{-1}) at 25 °C. It is also possible that the complex pattern of peaks could represent the sum of two or more conformations which are not interconverting on the NMR time scale.

A preliminary study of the line broadening for Cu^{I}(*trans*-cyhx-[14]aneS$_4$) was undertaken using the doublet at 3.45 ppm based on its ease of deconvolution. In order to examine the extent of line broadening in this experiment, three solutions were prepared spanning a wide concentration range with [$Cu^{II}L$] values of 0.030, 0.18, and 5.0 mM, the maximum concentration being limited by the $Cu^{II}L$ solubility in D_2O. The line width change at 25 °C was not statistically significant over this range, and it was concluded that the k_{11} value was too small to be measured on the NMR time scale. This suggests an upper limit of $k_{11} \leq 10^3$ M^{-1} s^{-1}.

Stopped-Flow Kinetic Measurements. All cross-reactions were studied in aqueous solution using stopped-flow spectrophotometry. The generalized reaction is represented in eq 3

$$Cu^{II}L + A_{Red} \underset{k_{21}}{\overset{k_{12}}{\rightleftharpoons}} Cu^{I}L + A_{Ox} \qquad (3)$$

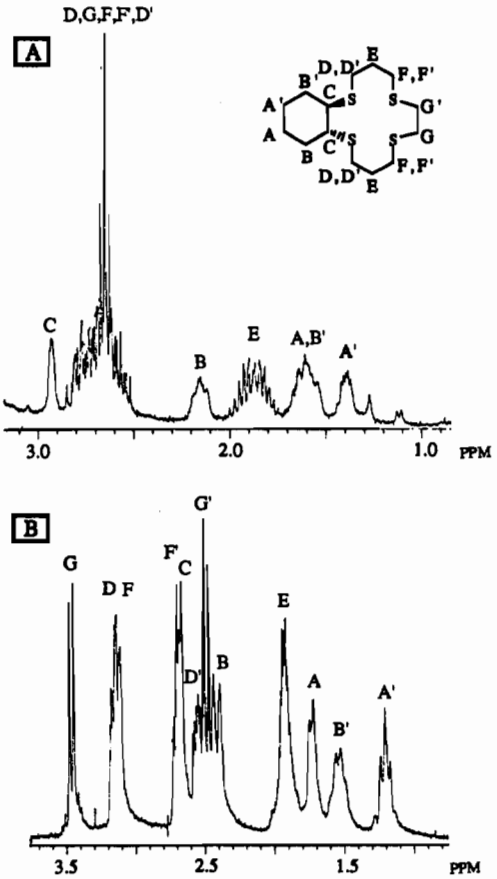

Figure 3. (A) ^{1}H-NMR spectrum for uncomplexed *trans*-cyhx-[14]aneS$_4$ in CD_3OD. (B) ^{1}H-NMR spectrum for Cu^{I}(*trans*-cyhx-[14]-aneS$_4$) in D_2O. Spectral assignments were made by analogy to the *cis*-cyhx-[14]aneS$_4$ system.

where k_{12} and k_{21} are defined as the second-order rate constants for $Cu^{II}L$ reduction and $Cu^{I}L$ oxidation, respectively. Both $Cu^{II/I}$(*cis*-) and $Cu^{II/I}$(*trans*-cyhx-[14]aneS$_4$) were reacted with five reducing agents (A_{Red}), $Ru^{II}(NH_3)_5$py, $Ru^{II}(NH_3)_5$isn, $Ru^{II}(NH_3)_4$bpy, $Ru^{II}(NH_3)_4$phen, and $Co^{II}(bpy)_3$, and three oxidizing agents (A_{Ox}), Ni^{III}([14]aneN$_4$)$(H_2O)_2$, $Ru^{III}(NH_3)_2(bpy)_2$, and Fe^{III}(4,7-Me$_2$phen)$_3$.[25] The formal potentials, self-exchange rate constants (k_{22}), and contact radii (r) for these counter-reagents have been given previously[7-9] except for $Co^{III/II}(bpy)_3$, for which $E^{\dagger} = 0.370$ V (vs NHE), $k_{22} = 17$ M^{-1} s^{-1}, and $r = 7.0 \times 10^{-8}$ cm.[26]

All reactions were found to be first-order with respect to each of the reactants except for the oxidation reactions with Ni^{III}-([14]aneN$_4$), as noted below. Most reactions were carried out under conditions where the concentrations of both reactants were within the same order of magnitude using the standard integrated second-order equation.[27] A few reactions were studied under

(25) Ligand abbreviations are as follows: py = pyridine, isn = isonicotinamide, bpy = 2,2′-bipyridine, phen = 1,10-phenanthroline, [14]-aneN$_4$ = 1,4,8,11-tetraazacyclotetradecane (cyclam), 4,7-Me$_2$phen = 4,7-dimethyl-1,10-phenanthroline.

(26) Tsukahara, K.; Wilkins, R. G. *Inorg. Chem.* **1985**, *24*, 3399−3402.

(27) For the cross-reactions utilizing the last two reagents listed in Table 4, the second-order rate constants exceeded 10^7 M^{-1} s^{-1}. However, from comparative studies using a trial program [Dunn, B. C.; Rorabacher, D. B. To be submitted for publication] based on a recently developed sophisticated treatment for very rapid second-order stopped-flow reactions [Meagher, N. E.; Rorabacher, D. B. *J. Phys. Chem.* **1994**, *98*, 12590−12593], we have ascertained that even the standard second-order treatment appeared to yield rate constants which are accurate within a factor of 2 or 3 even for reactions with half-lives as short as 0.5 ms when run on our fastest stopped-flow instrument (filling time = 3.8 ms).

Table 4. Second-Order Electron-Transfer Rate Constants Obtained for Reactions of $Cu^{II/I}$(*cis*-cyhx-[14]aneS$_4$) and $Cu^{II/I}$(*trans*-cyhx-[14]aneS$_4$) in Aqueous Solution at 25 °C and μ = 0.10 M (ClO_4^-) and Calculated Self-Exchange Rate Constants

	k_{12} (or k_{21}) × 10^{-6}, M^{-1} s^{-1}		calcd log k_{11} (M^{-1} s^{-1})	
	cis-cyhx-[14]aneS$_4$	*trans*-cyhx-[14]aneS$_4$	*cis*-cyhx-[14]aneS$_4$	*trans*-cyhx-[14]aneS$_4$
NMR relaxation			4.70	≤3
reductants				
$Ru^{II}(NH_3)_4$bpy	0.40 ± 0.10	0.29 ± 0.02	4.60	3.20
$Ru^{II}(NH_3)_4$phen	0.42 ± 0.20	0.36	4.4	3.2
$Ru^{II}(NH_3)_5$isn	0.88 ± 0.32	0.97 ± 0.37	4.19	3.33
$Ru^{II}(NH_3)_5$py	2.5 ± 1.5	1.6 ± 0.7	4.13	2.80
$Co^{II}(bpy)_3$	0.023	0.0005	4.8	3.1
oxidants				
$Ni^{III}([14]aneN_4)(H_2O)_2$				
pathway A	[7 ± 15]	0.4 ± 0.1	[4.5]	2.6
pathway B	0.35 ± 0.04	0.175 ± 0.007	1.6	1.8
$Ru^{III}(NH_3)_2(bpy)_2$	10 ± 4	5 ± 1	0.9	1.0
Fe^{III}(4,7-Me_2phen)$_3$	44 ± 10	15 ± 3	1.0	0.8

Table 5. Experimentally Observed Cross-Reaction Rate Constants for the Oxidation of Cu^I(*cis*-cyhx-[14]aneS$_4$) and Cu^I(*trans*-cyhx-[14]aneS$_4$) by Ni^{III}(cyclam) as a Function of Reagent Concentration in Aqueous Solution at 25 °C, μ = 0.10 M (ClO_4^-)

[Ni^{III}([14]-aneN$_4$)], mM	k_{obs}, s^{-1}	k_{21}(calcd) × 10^{-5}, M^{-1} s^{-1}	[Ni^{III}([14]-aneN$_4$)], mM	k_{obs}, s^{-1}	k_{21}(calcd) × 10^{-5}, M^{-1} s^{-1}
		Cu^I(*cis*-cyhx-[14]aneS$_4$)			
		Series I: [Cu^IL] = 12.01 μM			
0.0841	123	14.7	0.421	301	7.15
0.198	160	8.07	0.514	306	5.97
0.297	222	7.48			
		Series II: [Cu^IL] = 30.0 μM			
0.211	167	7.92	0.649	321	4.94
0.332	208	6.27	0.865	405	4.68
0.432	263	6.07			
		Series III: [Cu^IL] = 29.3 μM			
0.0737	91.6	12.44	0.461	266	5.78
0.166	162	9.73	0.770	387	5.02
0.310	214	6.90			
		Cu^I(*trans*-cyhx-[14]aneS$_4$)			
		Series I: [Cu^IL] = 7.44 μM			
0.0392	15.4	3.93	0.130	45.4	3.49
0.0627	26.1	4.16	0.194	54.9	2.84
0.0900	32.2	3.58	0.251	63.5	2.53
0.114	41.2	3.62	0.310	83.1	2.68
		Series II: [Cu^IL] = 13.9 μM			
0.164	49.3	3.00	0.884	158	1.79[a]
0.441	103.	2.34	1.145	210	1.83[a]
0.606	134	2.21	1.64	313	1.91[a]

[a] Value omitted from data resolution in Figure 9 since $k_{21} \approx k_{2B}$.

pseudo-first-order conditions in which the counterreagent was kept in large excess. For the reduction reactions, only two or three different concentrations were used for each specific reaction studied since the large number of cross-reactions provided ample checks on the veracity of the data. For the oxidation reactions, more extensive concentration studies were utilized due to the variable oxidation behavior. For each set of concentrations used, approximately 10 duplicate kinetic runs were made and the resolved cross-reaction rate constants were statistically averaged. The average values of k_{12} and k_{21} obtained for all reactions studied are listed in Table 4.

For the oxidation of Cu^I(*cis*-) and Cu^I(*trans*-cyhx-[14]aneS$_4$) by Ni^{III}([14]aneN$_4$), the kinetics were examined over a fairly wide range of Ni(III) reagent concentrations. All reactions with this reagent were run under pseudo-first-order conditions, for which the experimentally observed pseudo-first-order rate constants and calculated "apparent" second-order rate constants are listed in Table 5. (The stopped-flow instrument used has a filling time of 3.8 ms and has been shown to be capable of measuring first-order rate constants up to 300 s^{-1} without the introduction of significant error.) For both Cu^IL complexes reacting with the Ni(III) reagent, the calculated k_{21} values decrease with increasing Ni(III) concentration—a phenomenon which is indicative of the onset of rate-limiting conformational change or "gated" electron transfer.[7-9]

Rapid-Scan Cyclic Voltammetric Measurements. Cyclic voltammograms of solutions initially containing either $Cu^{II}L$ or Cu^IL in 80% methanol were obtained at 25 °C, over a scan range of $0.01-10^3$ V s^{-1}. The upper limit in accessible scan rate was generally imposed by the development of large background currents relative to the small signal. As has been previously described,[11] the changing patterns of the anodic and cathodic peaks and their relative amplitudes as a function of scan rate were used to generate initial estimates of all rate and equilibrium constant parameters based on Nicholson and Shain's theoretical treatments.[28] The values of these parameters were then further refined by computer simulation using a commercial version (DigiSim: Bioanalytical Systems, Lafayette, IN) of Rudolph's accelerated algorithm[29] based on Feldberg's finite difference method.[30] The initial parameters were adjusted until the trends in simulated behavior most closely matched the experimental voltammograms. The initial and refined values of all parameters are listed in Table 6, where $k_{s,OP}$ and $k_{s,QR}$ represent the heterogeneous rate constants for pathways A and B, respectively. Of the remaining five independent parameters, k_{OQ}, k_{QO}, k_{PR}, and k_{RP} represent the rate constants for individual conformational changes as defined by Scheme 1 and E_K^f is the redox potential for the overall half-reaction[11,31]

$$Cu^{II}L(O) + e^- \rightleftharpoons Cu^IL(R) \qquad E_K^f$$

The latter values are approximately 0.10 V higher than the corresponding E^f values in Table 1, a typical shift for $Cu^{II/I}L$ potentials as measured in 80% methanol and in water.[12] The other parameters listed are derived from the foregoing values where $K_{OQ} = k_{OQ}/k_{QO}$ and $K_{RP} = k_{RP}/k_{PR}$ represent the equilibrium constants for the formation of the Q and P intermediate species, respectively, and E_{OP}^f and E_{QR}^f represent the micro-

(28) Nicholson, R. S.; Shain, I. *Anal. Chem.* **1964**, *36*, 706-723. Cf.: (a) Nicholson, R. S. *Anal. Chem.* **1965**, *37*, 667-671. (b) Nicholson, R. S. *Anal. Chem.* **1966**, *38*, 1406.

(29) (a) Rudolph, M.; Reddy, D. P.; Feldberg, S. W. *Anal. Chem.* **1994**, *66*, 589A-600A. (b) Rudolph, M. *J. Electroanal. Chem. Interfacial Electrochem.* **1991**, *314*, 13-22. (c) Rudolph, M. *J. Electroanal. Chem. Interfacial Electrochem.* **1992**, *338*, 85-98.

(30) (a) Feldberg, S. W. *J. Electroanal. Chem. Interfacial Electrochem.* **1981**, *127*, 1-10. (b) Feldberg, S. W. *J. Electroanal. Chem. Interfacial Electrochem.* **1987**, *222*, 101-106. (c) Feldberg, S. W. In *Electroanalytical Chemistry. A Series of Advances*; Bard, A. J., Ed.; Marcel Dekker: New York, 1969; Vol. 3, pp 199-296.

(31) Laviron, E.; Roullier, L. *J. Electroanal. Chem. Interfacial Electrochem.* **1985**, *186*, 1-15.

Table 6. Estimated Parameters for the $Cu^{II/I}$(*cis*-cyhx-[14]aneS$_4$) and $Cu^{II/I}$(*cis*-cyhx-[14]aneS$_4$) Redox Couples As Determined from Rapid-Scan Cyclic Voltammetry in 80% Methanol at 25 °C, μ = 0.5 M ($NaNO_3$)[a]

	cis-cyhx-[14]aneS$_4$		*trans*-cyhx-[14]aneS$_4$	
parameter	initial est[b]	refined est[c]	initial est[b]	refined est[c]
E_K^f, V[d]	0.65	0.65	0.71	0.70
E_{OP}^f, V[d]	0.55	0.55	0.55	0.55
E_{QR}^f, V[d]	0.90	0.95	0.90	0.93
$k_{s,OP}$, cm s^{-1}	0.50	0.38	0.50	0.30
$k_{s,QR}$, cm s^{-1}	0.30	0.12	0.30	0.20
K_{RP}	2.1×10^{-2}	2.0×10^{-2}	2.0×10^{-3}	1.9×10^{-3}
K_{OQ}	5.9×10^{-5}	8.5×10^{-6}	4.9×10^{-4}	2.0×10^{-4}
k_{PR}, s^{-1}	2.2×10^4	2.2×10^4	2.0×10^5	8.0×10^4
k_{RP}, s^{-1}	4.6×10^2	4.4×10^2	3.9×10^2	1.5×10^2
k_{OQ}, s^{-1}	1.5	1.0	51	10
k_{QO}, s^{-1}	2.5×10^4	1.1×10^5	1.0×10^5	5.0×10^4

[a] All parameters referenced to Scheme 1. [b] Initial estimates were obtained by application of Nicholson and Shain's theory[28] to the relative changes in peak positions and magnitudes as a function of sweep rate in the experimental cyclic voltammograms. [c] Refined estimates were generated by adjusting the initial estimates to provide the best overall match between computer-simulated and experimentally obtained cyclic voltammograms with changing sweep rate (see text). [d] Potential values are referenced to aqueous NHE.

scopic potentials for O ⇌ P and Q ⇌ R:[31]

$$E_{OP}^f = E_K^f - (RT/n\mathcal{F}) \ln[(1 + K_{RP}^{-1})/(1 + K_{OQ})] \approx E_K^f + (RT/n\mathcal{F}) \ln K_{RP} \quad (4)$$

$$E_{QR}^f = E_K^f - (RT/n\mathcal{F}) \ln[(1 + K_{RP})/(1 + K_{OQ}^{-1})] \approx E_K^f - (RT/n\mathcal{F}) \ln K_{OQ} \quad (5)$$

It should be noted that the specific values listed for k_{OQ}, k_{QO}, and K_{OQ} are very rough approximations due to the fact that the intermediate Q was never observed as a dominant species.

Crystallographic Structural Determinations. Crystal structures were determined for both the Cu(II) and Cu(I) complexes of the *trans*-cyhx-[14]aneS$_4$ complex, the oxidized form being resolved both as a chloride and as a perchlorate salt. For the *cis*-cyhx-[14]aneS$_4$ system, only the Cu(II) complex was obtained in a crystalline form suitable for X-ray diffraction measurements. The atomic positional parameters for [Cu^{II}(*cis*-cyhx-[14]aneS$_4$)(H_2O)](ClO_4)$_2$ (**1**), [Cu^{II}(*trans*-cyhx-[14]aneS$_4$)(H_2O)](ClO_4)$_2$ (**2a**), [Cu^{II}(*trans*-cyhx-[14]aneS$_4$)Cl]·$^1/_2CuCl_4$·H_2O (**2b**), and [Cu^{I}(*trans*-cyhx-[14]aneS$_4$)]ClO_4·$^1/_4H_2O$ (**3**) are provided in the Supporting Information. Diagrams of the cationic units in these four structures along with the atom-labeling schemes are shown in Figures 4−7, respectively. In comparing the crystal structures, it should be noted that S1 and S2 are interconvertible as are S3 and S4, since each structure exists as a pair of optical isomers within the centric unit cell. For all four structures, selected bond lengths and bond angles are presented in Table 7. (Complete listings of all bond lengths and angles and all torsion angles for the cationic units are provided in the Supporting Information.)

The structure of [Cu^{II}(*cis*-cyhx-[14]aneS$_4$)(H_2O)](ClO_4)$_2$ (**1**) consists of a well-behaved cation, an ordered perchlorato anion, and one disordered perchlorato anion. The disordered anion was handled by assigning a number of partial oxygen atoms around Cl2 and refining them isotropically. All atoms occupy general positions in the unit cell. The S_4 base is ruffled, adjacent sulfur atoms being displaced ±0.24 Å from the average basal plane. The copper atom is located 0.28 Å above the best least-squares S_4 plane toward the apical oxygen atom. The Cu−S bond lengths average 2.321(8) Å and the Cu−O distance is 2.180(5) Å.

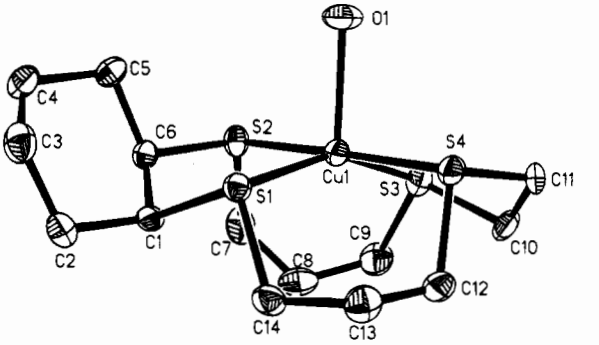

Figure 4. Molecular diagram of the cationic unit in the crystal structure of [Cu^{II}(*cis*-cyhx-[14]aneS$_4$)(H_2O)](ClO_4)$_2$ showing the atom-labeling scheme. The copper atom is positioned 0.28 Å above the average basal plane of the four sulfur donor atoms. The apically coordinated oxygen atom is from a water molecule. Two perchlorate anions, which are included in the unit cell, are not shown.

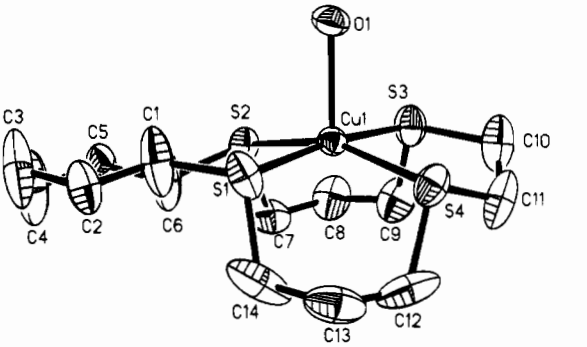

Figure 5. Molecular diagram of the cationic unit in the crystal structure of [Cu^{II}(*trans*-cyhx-[14]aneS$_4$)(H_2O)](ClO_4)$_2$ showing the atom-labeling scheme. The copper atom is positioned 0.28 Å above the average basal plane of the four sulfur donor atoms. The apically coordinated oxygen atom is from a water molecule. Two perchlorate anions, which are included in the unit cell, are not shown.

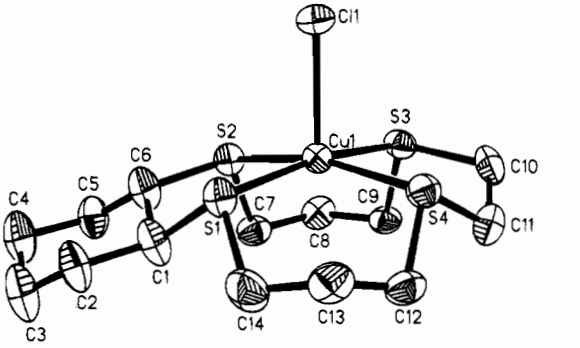

Figure 6. Molecular diagram of the cationic unit in the crystal structure of [Cu^{II}(*trans*-cyhx-[14]aneS$_4$)Cl]·$^1/_2CuCl_4$·H_2O showing the atom-labeling scheme. The copper atom is positioned 0.26 Å above the plane of the four sulfur donor atoms with an apically coordinated chloride ion. The unit cell also includes half a $CuCl_4^{2-}$ anion, which is not shown.

The structure of [Cu^{II}(*trans*-cyhx-[14]aneS$_4$)(H_2O)](ClO_4)$_2$ (**2a**) is similar to that of **1** consisting of a cation, one ordered anion, and one disordered anion. The disordered perchlorate region showed two separate sets of oxygen positions around Cl1, so two sets of four oxygen atoms were placed at 40% and 60% occupancies, respectively. All atoms occupy general positions in the unit cell. The S_4 plane is ruffled to a lesser degree than in **1** with each sulfur atom deviating ±0.14 Å from the average plane. The copper atom is again displaced 0.28 Å from the best least-squares S_4 plane toward the apical water ligand. The carbon atoms in the *trans*-cyhx-[14]aneS$_4$ ligand exhibit substantial thermal parameters, indicating disorder in

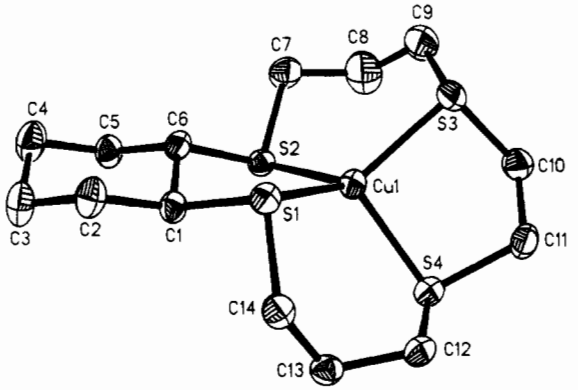

Figure 7. Molecular diagram of the cationic unit in the crystal structure of $[Cu^{I}(trans\text{-cyhx-}[14]aneS_4)]ClO_4 \cdot {}^1/_4H_2O$ showing the atom-labeling scheme. The copper is tetrahedrally coordinated to the four sulfur donor atoms. The perchlorate anion and one-quarter water molecule which are included within the unit cell are not shown.

Table 7. Selected Bond Lengths and Bond Angles for the Cationic Units in the Crystal Structures of $Cu^{II}(cis\text{-cyhx-}[14]aneS_4)(H_2O)](ClO_4)_2$ (**1**), $Cu^{II}(trans\text{-cyhx-}[14]aneS_4)(H_2O)](ClO_4)_2$ (**2a**), $Cu^{II}(trans\text{-cyhx-}[14]aneS_4)Cl] \cdot {}^1/_2CuCl_4 \cdot H_2O$ (**2b**), and $Cu^{I}(trans\text{-cyhx-}[14]aneS_4)]ClO_4 \cdot {}^1/_4H_2O$ (**3**)

Bond Lengths

	1	**2a**	**2b**	**3**
Cu1−S1	2.327(2)	2.301(3)	2.309(1)	2.259(1)
Cu1−S2	2.319(2)	2.310(2)	2.335(1)	2.254(1)
Cu1−S3	2.328(2)	2.315(3)	2.339(1)	2.257(1)
Cu1−S4	2.311(2)	2.308(2)	2.317(1)	2.276(1)
Cu1−O1/Cl1	2.180(5)	2.183(4)	2.458(1)	

Bond Angles

	1	**2a**	**2b**	**3**
S1−Cu1−S2	89.83(6)	89.53(8)	87.86(4)	95.42(4)
S2−Cu1−S3	90.08(6)	88.99(8)	87.12(4)	111.48(4)
S3−Cu1−S4	88.98(6)	90.11(8)	88.30(4)	95.58(5)
S4−Cu1−S1	90.26(6)	88.65(8)	93.92(5)	112.69(4)
S1−Cu1−S3	153.96(8)	172.61(8)	168.81(5)	126.17(5)
S2−Cu1−S4	178.03(7)	158.81(7)	164.45(5)	117.18(5)
S1−Cu1−O1/Cl1	102.3(1)	96.0(2)	95.32(4)	
S2−Cu1−O1/Cl1	89.6(1)	98.6(1)	100.81(4)	
S3−Cu1−O1/Cl1	103.8(1)	91.4(2)	95.44(4)	
S4−Cu1−O1/Cl1	92.3(1)	102.6(1)	94.42(4)	

their conformations. The average Cu−S bond distance is 2.309(6) Å and Cu−O = 2.183(4) Å.

In $[Cu^{II}(trans\text{-cyhx-}[14]aneS_4)(Cl)] \cdot {}^1/_2CuCl_4 \cdot H_2O$ (**2b**), the copper atom is displaced 0.26 Å from the S_4 basal plane and the four sulfur atoms are planar to within 0.04 Å. In the cation, the Cu−S distances average 2.325(14) Å and Cu−Cl = 2.458(1) Å. In the anion, Cu−Cl = 2.25(2) Å on average. The anion occupies a crystallographic 2-fold axis in the unit cell.

In the structure of $[Cu^{I}(trans\text{-cyhx-}[14]aneS_4)]ClO_4 \cdot {}^1/_4H_2O$ (**3**), the copper(I) ion is surrounded by a flattened tetrahedral arrangement of the sulfur atoms. The average Cu−S distance is 2.262(10) Å. The perchlorate is disordered, one oxygen being normal while the remaining three show two separate positions each. Atom O1 is assigned full occupancy as the apical atom in the perchlorate, and the other six oxygens are assigned $^1/_2$ occupancy. The solvent water molecule was assigned $^1/_4$ occupancy on the basis of an examination of its refined thermal parameters.

For all four crystal structures, the cyclohexane rings are in chair conformations. In the $Cu^{II}(trans\text{-cyhx-}[14]aneS_4)(OH_2)$ cation (**2a**), the torsion angles within the cyclohexane ring are decreased significantly, but this is always the result when thermal parameters are large and is not considered meaningful. Relative to the general S_4 plane in the current Cu(II) complexes, the C10−C11 ethylene bridge and the C1−C6 atoms of the bridging cyclohexane ring are skewed in the same direction (i.e., in a mirror image fashion) in structure **2b** (Figure 6) whereas they are twisted in opposite directions in structures **1** and **2a** (Figures 4 and 5). Since structures **2a** and **2b** differ in this regard, it is obvious that the direction of this skewing is not determined by the *cis* or *trans* orientation of the cyclohexane ring. As a result of its more symmetric skewing, the four sulfurs are more nearly planar in structure **2b**, as is evidenced by the near-equivalency of the S1−Cu1−S3 and S2−Cu1−S4 bond angles of 168.81 and 164.45°, respectively (Table 7). In structures **1** and **2a**, these two angles differ by 24 and 14°, respectively.

Discussion

Evaluation of Self-Exchange Rate Constants for Each Reaction Pathway. Application of the Marcus relationship[32] (including nonlinear and work term corrections)[7] to all cross-reaction rate constants obtained in the current study yields the self-exchange rate constant (k_{11}) values listed in the right two columns of Table 4. For each $Cu^{II/I}L$ system, all of the k_{11} values calculated from $Cu^{II}L$ reduction reactions ($k_{11(Red)}$) are seen to be consistent within experimental error and are in substantive agreement with the values ($k_{11(ex)}$) determined directly from the NMR line-broadening measurements. By contrast, the self-exchange rate constants calculated from the oxidation cross-reaction rate constants tend to be smaller and variable. This pattern of behavior indicates that pathway A (Scheme 1) is energetically preferred.[7-10] This assumption is corroborated by the data in Table 6 which clearly show that $K_{RP} \gg K_{OQ}$ for both systems included in this work; that is, intermediate P is significantly more stable than intermediate Q relative to their corresponding ground states. Since the self-exchange rate constants determined by NMR were obtained under conditions of zero driving force, $k_{11(ex)}$ must represent reaction via pathway A in Scheme 1. All *reduction* reactions must also be occurring by pathway A since a conformational change following the electron-transfer step will not become rate limiting for thermodynamically feasible reactions.[33] On this basis, we conclude that the $k_{11(A)}$ values for the *cis*- and *trans*-cyhx-[14]aneS$_4$ systems are approximately 5×10^4 and 2×10^3 M^{-1} s^{-1}, respectively. These values are compared with those for similar Cu(II/I) systems in Table 8.

For systems in which pathway A is preferred, $Cu^{I}L$ *oxidation* kinetics can be considerably more complex.[2,33] The complete oxidation rate constant expression[5b] can readily be simplified to the form[9]

$$k_{21} = \frac{k_{2A}k_{RP}}{k_{2A}[A_{Ox}] + k_{PR}} + k_{2B} \qquad (6)$$

where the two terms on the right represent the contributions of pathways A and B, respectively. When the k_{2B} term is negligible, eq 6 can be rearranged to the linear expression

$$\frac{1}{k_{21}} = \frac{[A_{Ox}]}{k_{RP}} + \frac{1}{k_{2A}K_{RP}} \qquad (6a)$$

By contrast, for conditions where k_{2B} may be significant but

(32) Marcus, R. A.; Sutin, N. *Biochim. Biophys. Acta* **1985**, *811*, 265−322.
(33) Brunschwig, B. S.; Sutin, N. *J. Am. Chem. Soc.* **1989**, *111*, 7454−7465.

Table 8. Comparative Self-Exchange Rate Constants for Pathways A and B and Rate Constants for the R → P Conformational Changes for $Cu^{II/I}$(*cis*-cyhx-[14]aneS$_4$) and $Cu^{II/I}$(*trans*-cyhx-[14]aneS$_4$) and Related Systems at 25 °C and μ = 0.10 M

complexed ligand	log $k_{11(A)}$ (M^{-1} s^{-1})[a]	log $k_{11(B)}$ (M^{-1} s^{-1})[b]	log k_{RP} (s^{-1})[c]	$k_{11(A)}/k_{11(B)}$
[13]aneS$_4$	5.5 ± 0.2[d]	≈2.0	≥2.3	≈3 × 10^3
[14]aneS$_4$	3.88 ± 0.09[d]	−0.1 ± 0.2	1.7 ± 0.1	1 × 10^4
syn-[14]aneS$_4$-diol	3.4 ● 0.1	−0.4 ± 0.3	2.20 ± 0.02	6 × 10^3
anti-[14]aneS$_4$-diol	4.3 ± 0.2	−2.0 ± 0.4	1.70 ± 0.03	2 × 10^6
cis-cyhx-[14]aneS$_4$	4.7 ± 0.3[d]	≈1	2.04 ± 0.03	≈5 × 10^3
trans-cyhx-[14]aneS$_4$	3.2 ± 0.2	≈1	1.51 ± 0.04	≈2 × 10^2
[15]aneS$_4$	4.08 ± 0.02[d]	≈2.2	≤0.7	≈8 × 10

[a] Values for $k_{11(A)}$ were taken from the average calculated $k_{11(Red)}$ values except as noted. [b] Values for $k_{11(B)}$ are estimated from the calculated $k_{11(Ox)}$ values for cross-reactions with the largest potential barrier functions. [c] Values for k_{RP} are calculated from oxidation reactions in which "gated" behavior was apparent. [d] Values for these specific systems are taken directly from NMR line-broadening measurements.

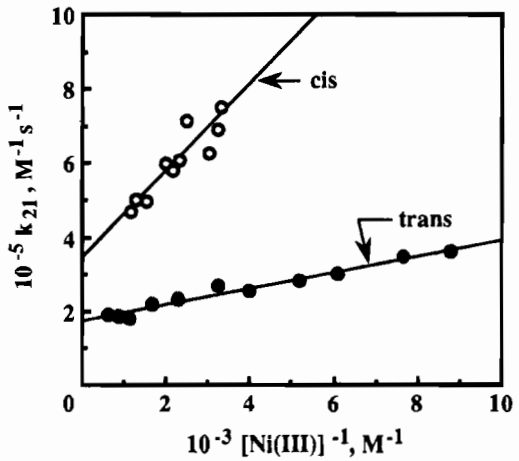

Figure 8. Pseudo-first-order rate constant data for the oxidation of both $Cu^{I}L$ species with excess Ni^{III}([14]aneN$_4$)(H$_2$O)$_2$ plotted according to eq 6b. The plot for the *cis* complex (open circles), based on data for [Ni(III)] ≥ 0.30 mM, yields k_{2B} = (3.56 ± 0.45) × 10^5 M^{-1} s^{-1} as the intercept and k_{RP} = 110 ± 19 s^{-1} as the slope. The plot for the *trans* complex (solid circles), based on data for [Ni(III)] ≥ 0.10 mM, yields k_{2B} = (1.75 ± 0.07) × 10^5 M^{-1} s^{-1} and k_{RP} = 22 ± 1 s^{-1}.

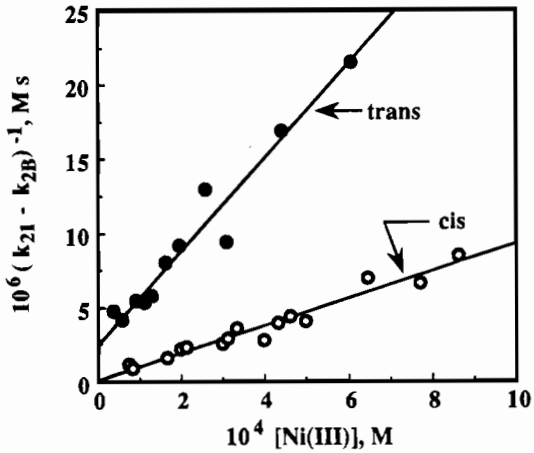

Figure 9. Pseudo-first-order rate constant data for the oxidation of both $Cu^{I}L$ species with excess Ni^{III}([14]aneN$_4$)(H$_2$O)$_2$ plotted in the form of eq 6c. The plot for the *cis* complex (open circles) is based on k_{2B} = 3.5 × 10^5 M^{-1} s^{-1} and yields a statistically meaningless value of $k_{21(A)}$ = (7 ± 15) × 10^6 M^{-1} s^{-1} as the reciprocal intercept and k_{RP} = 111 ± 8 s^{-1} as the reciprocal slope. The plot for the *trans* complex (solid circles) is based on k_{2B} = 1.75 × 10^5 M^{-1} s^{-1} and yields $k_{21(A)}$ = (4 ± 1) × 10^5 M^{-1} s^{-1} and k_{RP} = 32 ± 3 s^{-1}. The data for [Ni(III)] ≥ 0.8 mM were omitted from the *trans* plot since the term $k_{21} - k_{2B}$ is nearly negligible, leading to erroneous ordinate values.

$k_{PR} \ll k_{2A}[A_{Ox}]$

$$k_{21} = \frac{k_{RP}}{[A_{Ox}]} + k_{2B} \qquad (6b)$$

The $(k_{2A}K_{RP})^{-1}$ term on the right of eq 6a represents the value of $k_{21(A)}^{-1}$ for which species P and R are fully equilibrated so that $Cu^{I}L$ oxidation exhibits normal second-order behavior. However, as the concentration of A_{Ox} is increased (or as k_{2A} increases due to an increase in driving force or in the k_{22} value of the counterreagent), the *first* term on the right of eq 6a becomes increasingly important and may become dominant. When the latter condition occurs, the reaction will take on first-order character, independent of the oxidizing reagent concentration, permitting evaluation of k_{RP}, the rate constant for the conformational transformation of R to P. For large values of $[A_{Ox}]$, $(k_{2A}K_{RP})^{-1}$ becomes insignificant and eq 6b applies. Ultimately, the k_{2B} term, which represents the limiting second-order rate constant for pathway B ($k_{21(B)}$), should become dominant.

In the current study, the calculated k_{21} values for both $Cu^{I}L$ systems reacting with Ni^{III}([14]aneN$_4$) appear to decrease as the Ni(III) concentration increases (Table 5). A plot of either eq 6a or eq 6b exhibits curvature, indicating that all three rate constant terms in eq 6 are important over the range of concentrations studied. Therefore, the calculated k_{21} values for the highest Ni(III) concentrations were first plotted using eq 6b (Figure 8) and the k_{2B} value obtained from this intercept was subtracted from the k_{21} value for each specific kinetic run in plotting all of the Ni(III) data according to eq 6c. The

$$\frac{1}{k_{21} - k_{2B}} = \frac{[A_{Ox}]}{k_{RP}} + \frac{1}{k_{2A}K_{RP}} \qquad (6c)$$

resultant plots are shown in Figure 9, yielding $k_{21(A)} = k_{2A}K_{RP}$ as the reciprocal intercept and k_{RP} as the reciprocal slope. (In the case of the *trans*-cyhx derivative, kinetic data obtained for [Ni(III)] > 0.8 mM were omitted from Figure 9 since, for these conditions, $k_{21} \ll k_{2B}$, leading to very unreliable ordinate values.) In the case of the *cis*-cyhx-[14]aneS$_4$ system, the intercept in Figure 9 is not statistically significant so that a reliable $k_{21(A)}$ value could not be evaluated from the Ni(III) data for this system. The other $k_{21(A)}$ and $k_{21(B)}$ values derived from the Ni^{III}([14]aneN$_4$) kinetic data are given in Table 4 along with the corresponding self-exchange rate constants for the two pathways, $k_{11(A)}$ and $k_{11(B)}$, as calculated from application of the Marcus equation.

The plots in Figures 8 and 9 have well-defined slopes which should yield reliable values for k_{RP} (Table 8). The fact that these latter values are 4- to 5-fold smaller than the corresponding values calculated from the CV measurements (Table 6) are attributed to uncertainties in the CV data with a possible contribution from the different solvents used in the two methods. For the very fast oxidation reactions with Fe^{III}(4,7-Me$_2$phen)$_3$ and Ru^{III}(NH$_3$)$_2$(bpy)$_2$, the switch to pathway B is presumed to be complete. Application of the Marcus expression to these

cross-reaction rate constants yields essentially identical $k_{11(B)}$ values with both of these reagents, and these values are similar to those obtained from the Ni(III) oxidation studies at high Ni(III) concentration (Table 4). Since the oxidations with $Fe^{III}(4,7\text{-}Me_2phen)_3$ and $Ru^{III}(NH_3)_2(bpy)_2$ resulted in cross-reaction rate constants approaching or exceeding 10^7 M^{-1} s^{-1}, this level of agreement is well within experimental error. We conclude that, for both Cu^I(*cis*-cyhx-[14]aneS$_4$) and Cu^I(*trans*-cyhx-[14]aneS$_4$), $k_{11(B)} \ll 10$ M^{-1} s^{-1}.

Microscopic Self-Exchange Rate Constants. As noted in the preceding section, the limiting $k_{21(A)}$ values are equal to $k_{2A}K_{RP}$. Similarly, it can be shown that $k_{11(A)} = k_{AA}K_{RP}$ where k_{AA} represents the microscopic electron self-exchange rate constant for the O/P redox couple:[11a]

$$*O + P \rightleftharpoons *P + O \qquad k_{AA}$$

Utilizing the K_{RP} values from Table 6 and the $k_{11(A)}$ values from Table 8, the k_{AA} values for the *cis*- and *trans*-cyhx-[14]aneS$_4$ systems are estimated to be 2.5×10^6 and 0.8×10^6 M^{-1} s^{-1}, respectively. (Similar values can also be calculated for k_{BB}, the self-exchange rate constant for the Q/R redox couple; however, the K_{OQ} values determined in this work are considered to be too unreliable to make such calculations meaningful.) Although the probable errors in our K_{RP} values lend some uncertainty to the calculated k_{AA} values, these equilibrium constants are certainly known within a factor of 2 or better. The similarity between these two k_{AA} values suggests that roughly the same reorganizational barrier accompanies the electron-transfer step itself for both systems despite the fact that the two $k_{11(A)}$ values differ by approximately 30-fold.

It is particularly significant that our calculated k_{AA} values are similar to the largest known self-exchange rate constant for an inorganic Cu(II/I) system, $k_{11} = 5 \times 10^5$ M^{-1} s^{-1}, as determined directly from NMR line broadening by Pulliam and McMillin for the $Cu^{II/I}$(TAAB) complex,[34] a system which is

Cu(TAAB) =

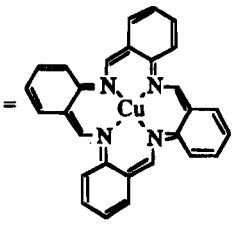

relatively rigid so that the reorganizational barrier accompanying electron transfer is presumed to be minimized. Recently reported self-exchange rate constants for the simple blue copper proteins (such as plastocyanin and azurin), as determined directly from NMR measurements, are also reported to be on the order of $(0.5-1) \times 10^6$ M^{-1} s^{-1}.[35,36] These latter values are particularly relevant since the type 1 copper sites in these proteins are considered to represent the archetypal example of copper systems whose conformations remain relatively constant during electron transfer.[37,38] Thus, we conclude that the $Cu^{II/I}$(*cis*-) and $Cu^{II/I}$(*trans*-cyhx-[14]aneS$_4$) systems involve only a minimal amount of reorganization *during the electron-transfer step itself*; but the *overall rate* of the electron-transfer process is reduced for these latter systems by the large conformational changes which occur sequentially with the electron-transfer step. The nature of this large conformational change is considered below.

Crystal Structures. As illustrated in Figures 4–6, the three $Cu^{II}L$ structures determined in the current work correspond to the so-called *trans* I (*RSRS* or + + + +) conformation[39–41] in which both trimethylene bridges are below the plane of the sulfur donor atoms, resulting in an overall "boat" conformation. As is generally the case in Cu(II) complexes of this type, there is only one apically coordinated donor atom, so that the complexes are five-coordinate, having a square pyramidal geometry with the copper atom displaced slightly above the basal plane in the direction of the apical group (water or chloride). The appearance of the *trans* I conformation in all three $Cu^{II}L$ crystal structures is particularly interesting since, in Cu(II) and Ni(II) complexes with unsubstituted [14]aneS$_4$ and [14]aneN$_4$, the so-called *trans* III (*RRSS* or + − − +)[39] conformation, in which the trimethylene bridges are on opposite sides of the donor atom plane to yield an overall "chair" conformation, is generally considered to be the most stable as determined by crystal structure determinations[42,43] and earlier molecular mechanics calculations.[44]

Square pyramidal structures of the type observed in the current work have been observed previously for Cu^{II}([12]aneS$_4$)(OH$_2$) and Cu^{II}([13]aneS$_4$)(OH$_2$).[45] However, these latter examples involve macrocycles having cavities which are too small to circumscribe the copper atom.[46] This limitation does not apply in the current study. The fact that the same structure is found for compounds **1**, **2a**, and **2b** suggests that the adoption of a square pyramidal geometry is independent of the strength of the apically coordinated donor atom or of the twist imposed upon the donor atoms by the cyclohexane ring.

(34) Pulliam, E. J.; McMillin, D. R. *Inorg. Chem.* **1984**, *23*, 1172–1175.
(35) (a) Groeneveld, C. M.; Canters, G. W. *J. Mol. Biol.* **1988**, *263*, 167–173. (b) Groeneveld, C. M.; Ouwerling, M. C.; Erkelens, C.; Canters, G. W. *J. Mol. Biol.* **1988**, *200*, 189–199.
(36) Comparisons between low molecular weight Cu(II/I) systems and Cu proteins should be undertaken only with great caution since the reactive centers in proteins may be separated by much greater distances and the high charges at the active patches may reduce close encounters during direct electron self-exchange measurements. On the other hand, low molecular weight Cu complexes are more susceptible to solvent reorganizational contributions than are the buried sites in proteins.
(37) (a) Guss, J. M.; Freeman, H. C. *J. Mol. Biol.* **1983**, *169*, 521–563. (b) Guss, J. M.; Harrowell, P. R.; Murata, M.; Norris, V. A.; Freeman, H. C. *J. Mol. Biol.* **1986**, *192*, 361–387.
(38) (a) Solomon, E. I.; Lowery, M. D. *Science* **1993**, *259*, 1575–1581 and references therein. (b) Adman, E. T. *Adv. Protein Chem.* **1991**, *42*, 142–197 and references therein.
(39) (a) Bosnich, B.; Poon, C. K.; Tobe, M. L. *Inorg. Chem.* **1965**, *4*, 1102–1108. (b) Curtis, N. F.; Swann, D. A.; Waters, T. N. *J. Chem. Soc., Dalton Trans.* **1973**, 1963–1974. (c) Wagner, F.; Mocella, M. T.; D'Aniello, M. J., Jr.; Wang, A. H.-J.; Barefield, E. K. *J. Am. Chem. Soc.* **1974**, *96*, 2625, 2627.
(40) The *trans* designation, as used to define conformational isomers in quadridentate macrocyclic ligand complexes, is based on the premise that two additional donor atoms from other ligands are also in the inner coordination sphere *trans* to each other. In the current $Cu^{II}L$ structures, there is no sixth donor atom, so that the *trans* designation is not completely appropriate in this sense. However, the same terminology has been used to define conformations for square planar structures, in which there are no apically-coordinated donor atoms. The *trans* designations can be applied equally well to square pyramidal complexes without ambiguity.
(41) The "*R*" and "*S*" designations refer to the chirality of the coordinated sulfur donor atoms in the order S1, S2, S3, S4 (i.e., positions 1, 4, 8, 11). The "+" and "−" designations refer to the orientation of the nonbonded lone pairs on the sulfur atoms relative to the S$_4$ plane, again in the order S1, S2, S3, S4.
(42) (a) Bosnich, B.; Mason, R.; Pauling, P. J.; Robertson, G. B.; Tobe, M. L. *Chem. Commun.* **1965**, 97–98. (b) Davis, P. H.; White, L. K.; Belford, R. L. *Inorg. Chem.* **1975**, *14*, 1753–1757.
(43) Glick, M. D.; Gavel, D. P.; Diaddario, L. L.; Rorabacher, D. B. *Inorg. Chem.* **1976**, *15*, 1190–1193.
(44) Brubaker, G. R.; Johnson, D. W. *Inorg. Chem.* **1984**, *23*, 1591–1595.
(45) Pett, V. B.; Diaddario, L. L., Jr.; Dockal, E. R.; Corfield, P. W. R.; Ceccarelli, C.; Glick, M. D.; Ochrymowycz, L. A.; Rorabacher, D. B. *Inorg. Chem.* **1983**, *22*, 3661–3670.
(46) Cooper, S. R.; Rawle, S. C. *Struct. Bonding (Berlin)* **1990**, *72*, 1–72.

In an earlier crystal structure of the parent $Cu^{I}([14]aneS_4)$ complex, one Cu−S bond was observed to rupture upon reduction of the copper complex[43] and the copper completed its coordination sphere by bonding to the free sulfur on an adjacent ligand to produce a polymeric structure with a 3:1 coordination array. The Cu^{I}(*trans*-cyhx-[14]aneS$_4$) structure reveals a distorted tetrahedral geometry with all four sulfurs coordinated to the copper atom (Figure 7), similar to the structure found previously for the $Cu^{I}([14]aneNS_3)$ complex.[47] We believe this is the dominant conformer in solution for all $Cu^{I}([14]aneS_4)$-type complexes.

An examination of the structural changes accompanying the reduction of $Cu^{II}L$ to $Cu^{I}L$, by a comparison of structures **2a** and **2b** with structure **3**, reveals that donor atoms S1 and S3 have inverted upon reduction of Cu(II) to Cu(I) as the ligand attempts to conform to a tetrahedral coordination geometry. The two trimethylene bridges have not changed their orientations relative to each other except for the fact that the central carbon in one bridge (C13) is puckered in the opposite direction in structure **3**. However, the S1−Cu1−S4 and S2−Cu1−S3 bond angles have opened by 11−12° while the other two angles (involving ethylene bridges) have opened only 5.5−6.5°. The opening of the former chelate angles is largely accomplished by a spreading of the S1−C14−C13 and S3−C9−C8 bond angles. The inability of the five-membered chelate rings to expand further appears to be a major factor in the overall flattening of the tetrahedral structure.

Assessment of Conformational Changes Accompanying Copper(II/I) Electron Transfer. From the data in Table 1,[12] it is apparent that the $Cu^{II}L$ complexes formed with the *cis*- and *trans*-cyhx-[14]aneS$_4$ ligands exhibit nearly identical stability constant values whereas, for the $Cu^{I}L$ species, the *trans* complex is approximately 10 times more stable than the *cis* complex. Interestingly, the K_{RP} value for the *trans* system is also 10 times larger than for the *cis* system. This observation, coupled with our conclusion above that only a minimal amount of reorganization accompanies the electron-transfer step itself, appears to be consistent with our earlier proposal that the P intermediate may be similar in conformation to the O species.[11b] Thus, the greater thermodynamic reorganization required for the R → P transition in the *trans* $Cu^{I}L$ complex, as reflected by K_{RP}, appears to be correlated to the greater stability of the R species.

As we recently discussed elsewhere,[13] internal strain calculations indicate that, for fully complexed $Cu^{II}([14]aneS_4)$ and its cyclohexanediyl derivatives, the conformer designated as *trans* I (*RSRS* or + + + +)[39,41] (i.e., the conformer found in crystal structures **1**, **2a**, and **2b**) is slightly more stable than the *trans* III conformer (*RRSS* or + − − +),[39] although both may exist in significant amounts in solution. Similar calculations reveal that the most stable conformation for the corresponding $Cu^{I}L$ complexes is the tetrahedral conformer found in crystal structure **3**. Therefore, we presume that the crystal structures determined in this work give a reasonably accurate view of the solution structures which correspond to the two stable species in Scheme 1, designated as $Cu^{II}L(O)$ and $Cu^{I}L(R)$.

As noted in the preceding section, the conversion of structure **2a** to structure **3** requires the inversion of two coordinated sulfur donor atoms. Assuming that these two inversions occur as discrete steps, the proposed stepwise mechanism can then be represented by the sequence shown in Figure 10—for which all of the conformations shown represent minimal strain structures as generated using the software Chem3D Plus (Cambridge Scientific Computing, Cambridge, MA). In this figure, species **A** corresponds to the *trans* I conformer in crystal structures **1**, **2a**, and **2b** while species **F** corresponds to the conformation in crystal structure **3**. Species **B** and **C** in Figure 10 represent metastable $Cu^{II}L$ conformations, commonly designated as the *trans* II (*RRRS* or + − + +)[39] and *trans* V (*RRRR* or + − + −)[39] conformers, respectively, of which species **C** is the most highly strained.[13] Similarly, species **D** and **E** represent the corresponding strained $Cu^{I}L$ conformers, of which the former is the least stable. We postulate that the metastable intermediates designated as $Cu^{II}L(Q)$ and $Cu^{I}L(P)$ in Scheme 1 are likely to resemble species **C** and **D**, respectively, in Figure 10. It follows that pathway A in Scheme 1 is represented by the sequence **A** ⇌ **D** ⇌ **E** ⇌ **F** while pathway B consists of the sequence **A** ⇌ **B** ⇌ **C** ⇌ **F**. Although these sequences imply the presence of two metastable intermediates along each pathway, it is unlikely that all intermediates would be kinetically observable since the sequential steps **A** ⇌ **B** and **B** ⇌ **C** (and, likewise, **C** ⇌ **D** and **D** ⇌ **E**) are both first-order processes whose relative rates could not be easily altered by the reaction conditions. Thus, we assume that the less strained intermediates, **B** and **E**, are transparent *vis-á-vis* the kinetic data. Figure 10 also suggests the possibility of a third reaction pathway represented by **A** ⇌ **B** ⇌ **E** ⇌ **F**, but for the reasons stated above, it is unlikely that more than two pathways will be kinetically distinguishable for any specific $Cu^{II/I}L$ system. At the very least, the conformers represented in Figure 10 provide a working hypothesis for examining the kinetic influences to be expected upon the introduction of various conformational constraints.

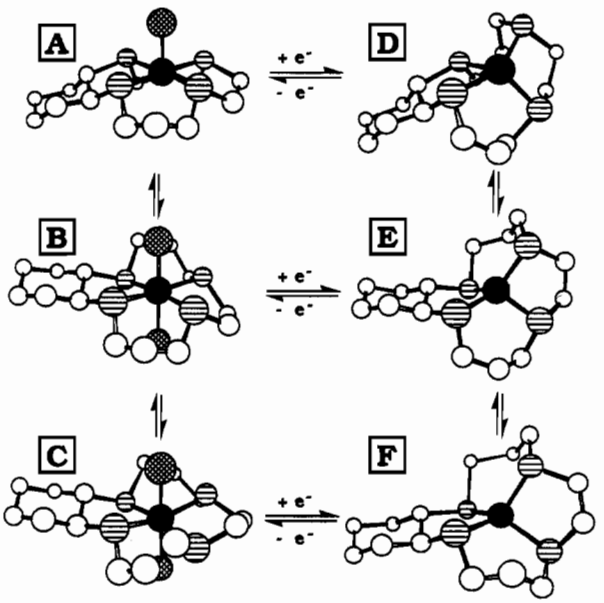

Figure 10. Proposed scheme for electron transfer involving $Cu^{II/I}$(*trans*-cyhx-[14]aneS$_4$) illustrating the sequential changes in configuration which may occur as discrete steps. The solid atoms represent copper, the striped atoms are sulfurs, and the cross-hatched atoms are coordinated solvent molecules. Species "**A**" (square pyramidal—*trans* I) and "**F**" (tetrahedral) represent the stable forms of $Cu^{II}L$ and $Cu^{I}L$ as revealed by the crystal structures shown in Figures 6 and 7. All other $Cu^{II}L$ species are shown with two apically coordinated solvent molecules although it is unclear whether one or two solvent molecules (or anions) may be coordinated in solution. The chirality of the sulfur donor atoms and the directionality of the sulfur lone-pair electrons are as follows (where the designations start with the S1 atom at left foreground and proceed clockwise):[39-41] species "**A**" (*trans* I) and "**D**", *RSRS* or + + + +; species "**B**" (*trans* II) and "**E**", *RRRS* or + − + +; species "**C**" (*trans* V) and "**F**", *RRRR* or + − + −.

(47) Bernardo, M. M.; Heeg, M. J.; Schroeder, R. R.; Ochrymowycz, L. A.; Rorabacher, D. B. *Inorg. Chem.* **1992**, *31*, 191−198.

Conclusions. In terms of the proposed stepwise mechanism depicted in Figure 10, the relative magnitudes of the $K_{Cu^{I}L}$ and K_{RP} values determined for the current *cis*- and *trans*-cyhx-[14]-aneS$_4$ systems suggest that, on a relative basis, species "**F**" is stabilized for the *trans*-cyhx-[14]aneS$_4$ system, requiring a larger reorganizational energy to form species "**D**" prior to the electron-transfer step. The rate constant for the microscopic electron self-exchange rate constant involving "**A**" and "**D**" (correlated to "O" and "P" in Scheme 1) appear to be similar for both systems and compare favorably to the largest self-exchange rate constants reported for rigid $Cu^{II/I}L$ systems. Thus, the portion of the overall reorganizational energy which is presumed to accompany the electron-transfer step itself is apparently quite small.

From the foregoing analysis, it is tempting to conclude that the energy barriers associated with sulfur atom inversions are responsible for the appearance of square-scheme behavior in the Cu(II/I) macrocyclic tetrathiaether systems. However, low-temperature cyclic voltammetric studies now in progress in our laboratories on $Cu^{II/I}L$ systems with tripodal ligands suggest the occurrence of metastable intermediates in the absence of donor atom inversion. Wilson and co-workers[48] have also observed square-scheme behavior in slow-scan cyclic voltammetric studies on the $Cu^{II/I}([9]aneS_3)_2$ system in which two Cu−S bonds rupture upon Cu(II) reduction without being accompanied by donor atom inversion. Thus, it is apparent that structural changes other than donor atom inversion can lead to similar dual-pathway behavior in Cu(II/I) systems.

Acknowledgment. Financial support of this research by the National Science Foundation (Grant CHE-9218391) is gratefully acknowledged.

Supporting Information Available: Tables of additional crystallographic data, thermal parameters, hydrogen parameters, atomic coordinates, complete bond lengths and bond angles, and torsion angles (23 pages). Ordering information is given on any current masthead page.

IC941187W

(48) Sanaullah; Kano,K.; Glass, R. S.; Wilson, G. S. *J. Am. Chem. Soc.* **1993**, *115*, 592−600.